MULTIFUNCTIONAL THIN FILM ASSEMBLIES ON PLASTIC FILM

Jaime C. Grunlan, Assistant Professor, Texas A&M University, College Station, TX.

Abstract

A variety of thin, functional coatings can be produced using layer-by-layer (LbL) assembly. Thin films, typically < 1μm thick, are created by alternately exposing a substrate to positively- and negatively-charged molecules or particles in water. This deposition process is repeated until the desired number of "bilayers" (or cationic-anionic pairs) is achieved. Several functionalities imparted to polymer films using this technique are described here. Coatings made from poly (diallyldimethylammonium chloride) and deoxycholate-stabilized carbon nanotubes are able to achieve an electrical conductivity of 100 S/cm, while remaining transparent at a thickness below 100 nm. UV-resistant thin films can be similarly produced using colloidal TiO_2 nanoparticles. Assemblies of natural sodium montmorrilonite clay and polyethylenimine, that are less than 300 nm thick, have been produced with an oxygen transmission rate below 0.005 cm^3/m^2/day (lower permeability than SiOx when OTR multiplied by thickness) due to a nano brick wall structure. These thin, transparent composites, containing up to 80 wt% clay, are a good candidate for foil replacement in food packaging and flexible electronics packaging. These same assemblies impart flame resistance to foam and fabric by coating them three-dimensionally. These assemblies can also be made antimicrobial by depositing in the presence of a biocidal agent (e.g., cetyltrimethylammonium bromide). All of the materials described are water-based and processing occurs under ambient conditions. By changing the types of polymers used, these films can also be made to exhibit a tacky behavior, which may be useful for pressure sensitive tapes.

1. Introduction

A variety of functional thin films can be produced using the layer-by-layer (LbL), or electrostatic self-assembly (ESA) technique [1-2], LbL-based thin films are currently being evaluated for a variety of applications that include drug delivery [3], molecular sensing [4], solid battery electrolyte [5], photovoltaics [6], membranes [7], anti-fungal [8], and flame retardance [9]. Thin films, typically < 1μm thick, are created by alternately exposing a substrate to positively- and negatively-charged molecules or particles, as shown in Figure 1. In this case, steps 1 – 4 are continuously repeated until the desired number of "bilayers" (or cationic-anionic pairs) is achieved. Each individual layer may be 1 – 100+ nm thick depending on chemistry, molecular weight, charge density, temperature, deposition time, counterion, and pH of species being deposited. The ability to control coating thickness down to the nm-level, easily insert variable thin layers without altering the process, economically use raw materials (due to thin nature), self-heal, and process under ambient conditions are some of the key advantages this deposition technique has. These films often have properties that are better than comparable thick films (>>1μm). Furthermore, these films are often transparent, which opens up areas of use not available to comparable bulk films. Altering the order and composition of layers provides limitless opportunity for new functionality. In the present work, LbL thin film assemblies that impart electrical conductivity [10-11], UV-resistance [12], antimicrobial behavior [13-14] and oxygen barrier [15-16] to plastic films are described.

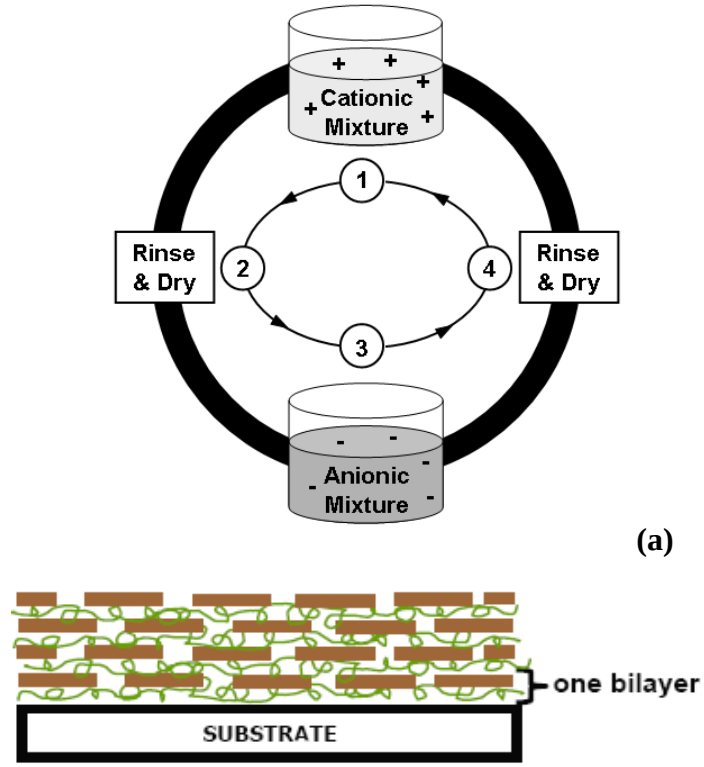

Figure 1. Schematic of the layer-by-layer self-assembly procedure for creating multifunctional thin films (a). Steps 1 – 4 are repeated to create a multilayer film on a substrate (b). This schematic is showing negatively-charged clay platelets deposited with a polycation, which generates a nano brick wall structure.

2. EXPERIMENTAL

2.1 Materials

For oxygen barrier assemblies, cationic branched polyethylenimine (PEI) (M_w = 25,000 g/mol and M_n = 10,000 g/mol) was purchased from Sigma-Aldrich (Milwaukee, WI). The pH of 0.1 wt. % PEI in deionized water was adjusted using 1 M HCl prior to film assembly. Southern Clay Products, Inc. (Gonzales, TX) supplied natural, untreated montmorillonite (MMT) (tradename Cloisite NA^+), and the pH of 0.2 wt. % MMT was unaltered. This clay has a reported cationic exchange capacity of 0.926meq/g and is negatively-charged in deionized water. MMT platelets have a reported density of 2.86 g/cm^3, diameter of 10-1000nm, and thickness of 1nm [17]. Polyethylene terephthalate (PET) film with a thickness of 179μm (trade name ST505, produced by DuPont-Teijin) was purchased from Tekra (New Berlin, WI) and used as the model substrate for OTR testing. This PET film has an OTR of approximately 8.6 cm^3/(m^2·day·atm) under dry conditions. Prior to coating, PET film was rinsed with deionized water, methanol, and again with water before being dried with filtered air. These substrates were then corona treated using a BD-20C Corona Treater (Electro-Technic Products, Inc., Chicago) to impart a negative surface charge [18-19]. Single-side-polished silicon wafers (University Wafers, South Boston, MA), 500μm in thickness, were used for film growth characterization by ellipsometry. For deposition onto silicon wafers, a 30–minute piranha treatment was performed [20]. [***Caution***: Piranha solution reacts violently with organic materials and should be handled with extreme caution.] Following treatment, substrates were initially dipped in the cationic solution for 5 minutes, followed by rinsing

with de-ionized water and blow drying with filtered air. The same procedure was followed with the clay solution, or negatively-charged polymer solution, to complete the first bilayer. Each subsequent bilayer was dipped for one minute in each given aqueous mixture.

Antimicrobial films were made from polyacrylic acid (PAA) (M_w = 100,000 g/mol), cetyltrimethylammonium bromide (CTAB), and polydiallyldimethylammonium chloride (PDDA) were purchased from Aldrich Chemical Co. (St. Louis, MO). Bacteria used for testing included Escherichia coli (*E. coli*) K-12, F galK16 galE15 relA1 rpsL150 spoT1 mcrB1 and Staphylococcus aureus (*S. aureus*), wild type strain. UV-protected films were made using an anionic deposition solution containing 0.3 wt% PEDOT-PSS (tradename BAYTRON P HC V4) that was purchased from H.C. Starck (Newton, MA). Cationic mixtures contained PEI. Carbon black with a 40 nm particle size, provided by Columbian Chemicals (Marietta, GA), or 10 nm TiO_2 provided by Applied NanoWorks (Watervliet, NY) were added to the cationic solution. When CB or TiO_2 were added, 0.05 wt% polymer was used with 0.25 wt% CB or TiO_2, otherwise the solution contained 0.3 wt% polymer.

For conductive thin films, three different types of nanotubes were purchased: multi-walled carbon nanotubes (MWNTs) [15 nm outer and 4 nm inner diameters and 1-10+ μm length, C ≥ 95 wt%] from Bayer MaterialScience, XM grade (a mixture of single, di- and tri-walled nanotubes) and purified high-pressure carbon monoxide process (HiPCO) single-walled carbon nanotubes (SWNTs) [1 nm diameter and 0.1-1 μm length, C ≥ 85 wt%] from Unidym Inc. The PDDA (described above) and sodium deoxycholate (DOC, C24H39NaO4, ≥ 98 %) were purchased from Aldrich. A 0.25 wt% PDDA aqueous solution was prepared as a cationic solution by dissolving in deionized water. The anionic solution was prepared by dissolving 0.05 wt% CNTs in deionized water, stabilized by 2 wt% DOC and followed by mild ultrasonicating for 20 min to remove large CNT bundles and impurities. All solutions were used in the state of their natural pH. Fused quartz slides (Structure Probe Inc.), silicon wafers (University Wafer) and PET films were used as deposition substrates for films characterized with UV-Vis, ellipsometry and micro-imaging, respectively. Also, PS films (Goodfellow) were cut to size and used for opto-electric property measurements.

2.2 Thin Film Deposition

Unless otherwise noted, all films were prepared according to the procedure outlined in Figure 1. The initial bilayer for each film was deposited by dipping a given substrate into each of the ionic solutions for 5 minutes, beginning with the cationic solution. Subsequent bilayers were deposited with one minute dips. Each dip was followed by rinsing with deionized water for 30 seconds and drying with filtered air for 30 seconds. Films with more than 10-bilayers were produced using home-built robots [21-22].

2.3 Characterization

All films created for oxygen transmission rate testing were sent to MOCON (Minneapolis, MN) and tested in accordance with ASTM D-3985 [23], using an Oxtran 2/21 ML instrument. OTR testing was done at 23°C and 0%RH, unless otherwise specified. Film thickness was measured on silicon wafers using a PHE-101 Discrete Wavelength Ellipsometer (Microphotonics, Allentown, PA) at a wavelength of 632.8 nm and a 65° incidence angle. Thin film cross sections were imaged using a JEOL 1200EX TEM (Parody, MA). Weight of each deposited layer was measured with a MAXTEX quartz crystal microbalance (QCM) and 5 MHz gold-electrode quartz crystals. The quartz crystals were cleaned with an oxygen plasma etcher. Scanning electron microscope (SEM) images were obtained with a JEOL JMS-6400 with an operating voltage of 100 kV. Absorbance and transmittance of deposited films on fused quartz slides were measured with a USB2000 UV-Vis spectrometer (Ocean Optics). To calculate

sheet resistance, voltage and current values were read using Signatone Pro4 Four-Point Probe (Tomkins CT.), E3644A DC Power Supply with an operating voltage of 10V (Agilent Technologies Inc.), and a Digital Multimeter (Keithley Instruments Inc.). Antimicrobial effectiveness was determined using a Kirby-Bauer test. In this test, films are deposited on PET and cut into disks. These are transferred onto plates of agar that were swabbed with a strain of bacteria. These plates were then incubated for 24 hours and examined to determine the hindrance of bacterial growth by measuring a zone of inhibition (ZOI). Film thickness of antimicrobial and PEDOT-based assemblies was measured with a Dektak Profilometer (Veeco Instruments Inc., Woodbury, NY). A UVP XX-15L bench lamp (Upland, CA) was used to expose films PEDOT-based assemblies to 365 nm light for UV degradation studies.

3. Results and discussion

3.1 Oxygen barrier of PEI-MMT

Figure 2 shows how the barrier of PEI-MMT films, deposited on PET, decreases with increasing space between clay layers. This alteration of clay spacing was achieved by changing the charge density of the PEI solution by adjusting its pH prior to deposition. PEI is highly charged at low pH and therefore deposits thinner (due to self repulsion) than when it is weakly charged at higher pH [16]. Ellipsometric thickness data reveal that films assembled with PEI at pH 7 have an average space between clay layers of 0.2 nm, which increases to 2.4 nm with PEI at pH 10. Figure 3 is a cross-sectional TEM image that clearly shows the orientation and structure of a PEI/MMT film. This 40-bilayer film, made with pH 10 PEI and MMT clay, shows every individual clay layer, explicitly proving the proposed nano brick wall structure. In this case, polystyrene was used as the substrate for deposition because it sections better in the microtome used to prepare TEM samples. The wrinkled surface is likely due to stress relaxation when the film is sectioned down to approximately 100 nm thick. More recently, undetectable oxygen transmission rates have been achieved with fewer than eight clay layers by further increasing the clay spacing. Crosslinking with glutaraldehyde has also helped to reduce moisture sensitivity of the oxygen barrier. All of these clay-based assemblies exhibit better than 90% visible light transmission between 400 and 800 nm.

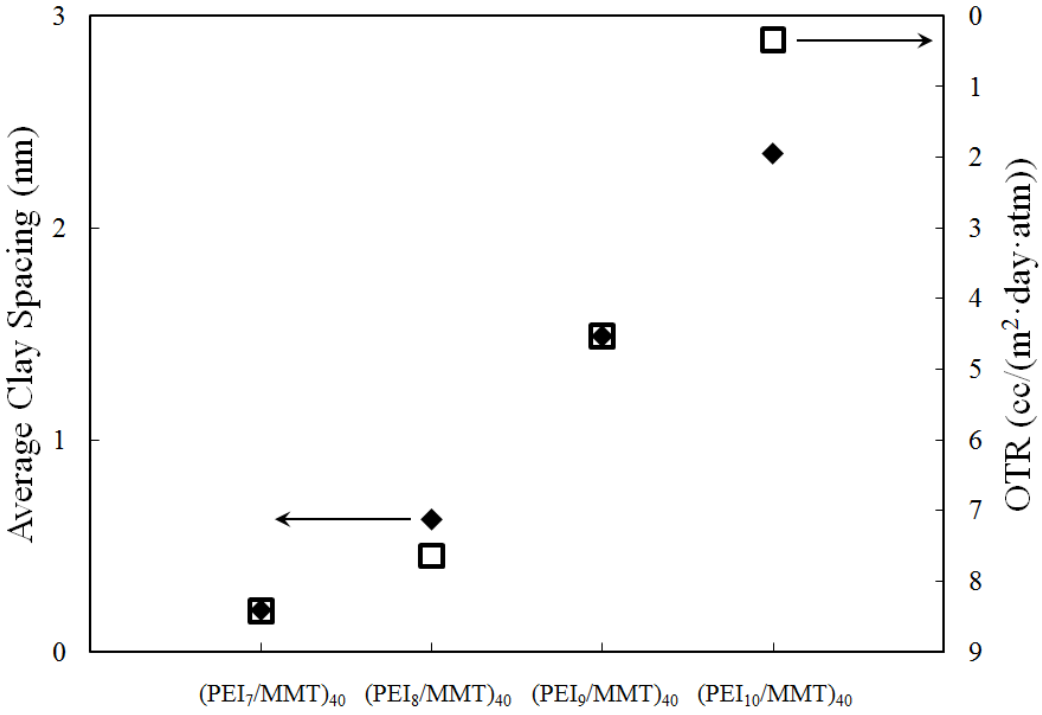

Figure 2. Oxygen transmission rate and average clay spacing as a function of PEI pH (adapted from Ref. 16).

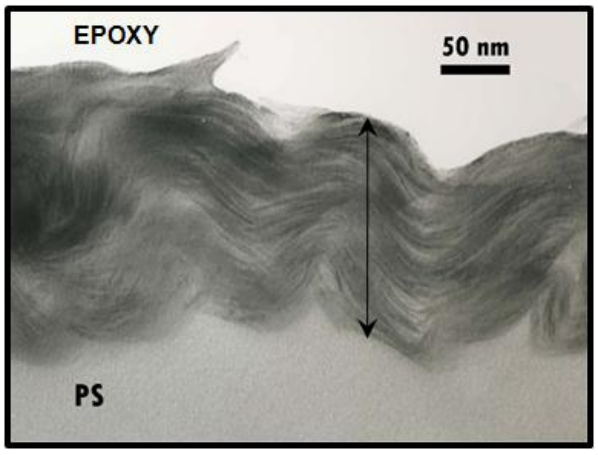

Figure 3. TEM image of a 40 bilayer film of PEI (pH 10)-MMT on polystyrene (adapted from Ref. 16).

3.2 Electrical conductivity of nanotube-based assemblies

Film growth and mass increase were analyzed every 2 bilayers using ellipsometry and QCM for three PDDA/(CNT+DOC) systems in Figure 4. Linear growth constitutes successful combination of PDDA and CNT within the film as well as constant deposition of both species up to 20 BLs [11]. The SWNT-based films grow thinner than MWNTs, suggesting that the film thickness depends on the radial size of each CNT. Similar to the ellipsometric film thickness, film mass increases linearly, suggesting constant deposition with the LbL assembly technique. With the average thickness of each

PDDA/(CNT+DOC) system, QCM mass data yield each film density as well as composition as weight percent. The amounts of PDDA and SWNT+DOC adsorbed onto the quartz crystal in each deposition cycle were estimated to be 0.037 and 0.35 μg/cm^2, respectively, in the inset of Fig. 2(b), showing that SWNT+DOC are depositing more than PDDA. Additionally, for all three systems, composition of CNTs was over 90 wt% throughout the 20 BL thin films. Because SWNT has a maximum density of 1.55 g/cm3 similar to PDDA (1.09 g/cm^3), SWNT contributes greater to weight per layer than PDDA. The $[PDDA/(SWNT+DOC)]_{20}$ film density is larger than PDDA or SWNT individually however, it is close to their sum of 2.64 g/cm^3, suggesting the result of a more ordered structure in the assembly. In two insets of Fig. 4, thickness increases after deposition of SWNT, while it slightly decreases after that of PDDA. However, mass increases even after deposition of PDDA, which suggests PDDA penetrating inand absorbing onto an underlying CNT layer to form a PDDA/(CNT+DOC) nanocomposite.

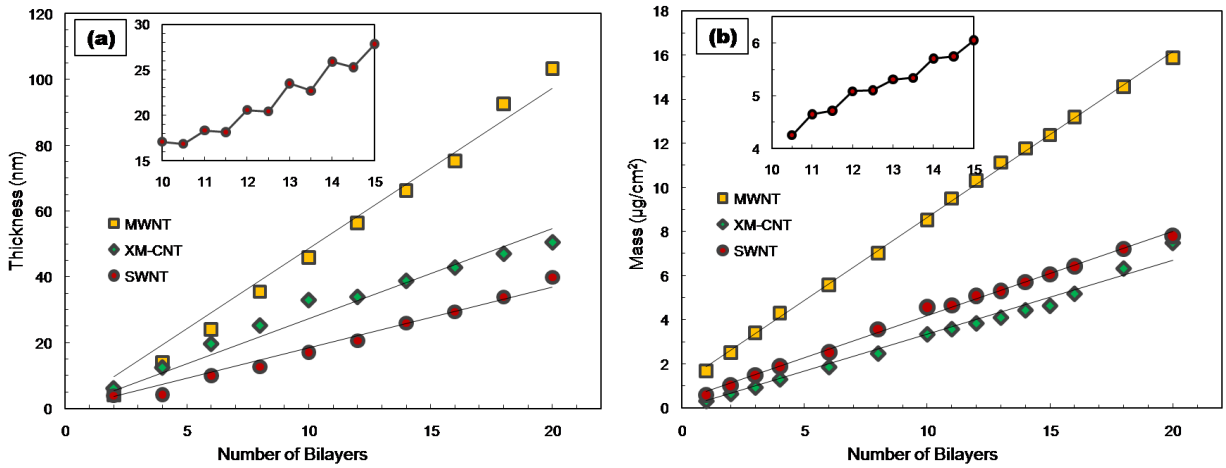

Figure 4. Film thickness (a) and mass growth (b) of three types of thin films as a function of the number of bilayers. Insets are data of a SWNT thin film from 10 to 15 BLs, where half of a bilayer corresponds to PDDA deposition (adapted from Ref. 11).

Figure 5 shows the electrical conductivity of $[PDDA/(CNT+DOC)]_n$ thin films as a function of the number of BLs up to 20, calculated from the sheet resistance and film thickness. $[PDDA/(SWNT+DOC)]_{20}$ thin films had conductivity of 148 S/cm (41.6 nm thick with a sheet resistance of 1.62 kΩ/sq) as well as 30 S/cm conductivity with just two BLs much higher than $[PDDA/(MWNT+DOC)]_n$ thin films [11]. In the SWNT thin film, the conductivity gradually increased from 30 to 150 S/cm as ~~increase of~~ the number of BLs increased, while the MWNT thin film has a constant conductivity. These characters of conductivity, the gradual increase vs. the steady state, can be explained through the nanostructure of two thin films. As more BL deposition, density of intersecting pathways can increase due to interconnection between SWNTs in upper and lower layers. In the MWNT films, homogeneous 3-dimensional MWNT networks can be readily formed in fewer BL due to the low aspect ratio, thus the density of intersecting pathways was not improved as the number of BL increased.

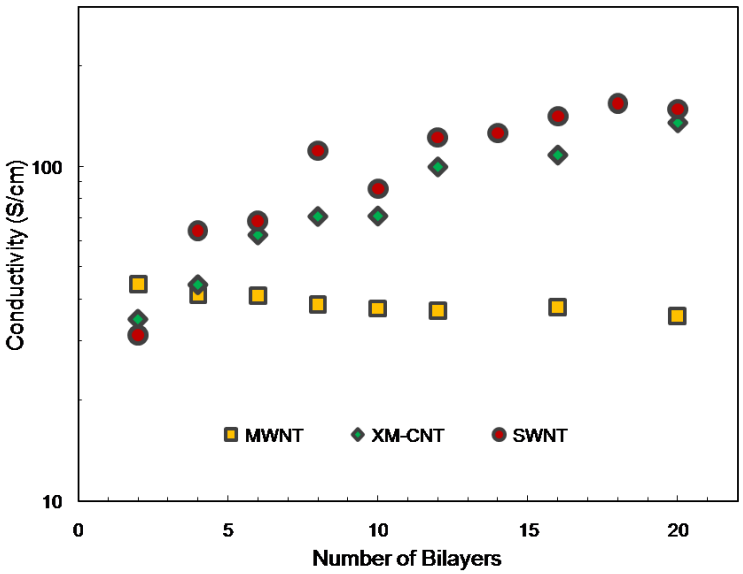

Figure 5. Electrical conductivity of three types of nanotube-based thin films up to 20 BLs (adapted from Ref. 11).

.

3.3 Antimicrobial behavior of assemblies containing quaternary ammonium surfactants

Film growth was monitored using QCM. A control system (without the antimicrobial agent) was analyzed for comparison. With the addition of CTAB, growth increases at a much higher rate than the PDDA/PAA control (Figure 6). Additionally, weight variation between PDDA+CTAB/PAA and the CTAB/PAA systems is minimal. Film thicknesses were evaluated using profilometry at 7, 10, 15, and 20 bilayers. The growth trend mimics the trend obtained using QCM. Since the PDDA/PAA films have a much slower growth rate, these were too thin for measurement using profilometry at less than 20 BL were not analyzed. Again, film growth in the CTAB/PAA system was greater than PDDA+CTAB/PAA, reaching approximately 4 μm at 20 BL. It has been shown that the addition of salts to solutions used in LbL yields thicker films [24]. In this system, the CTAB acts as a salt, screening the charge and thus yielding a much thicker film. Similarly, when the PDDA is removed from the cationic solution, the charge density decreases, and the resulting film is slightly thicker. However, this decreased charge density makes the film rougher.

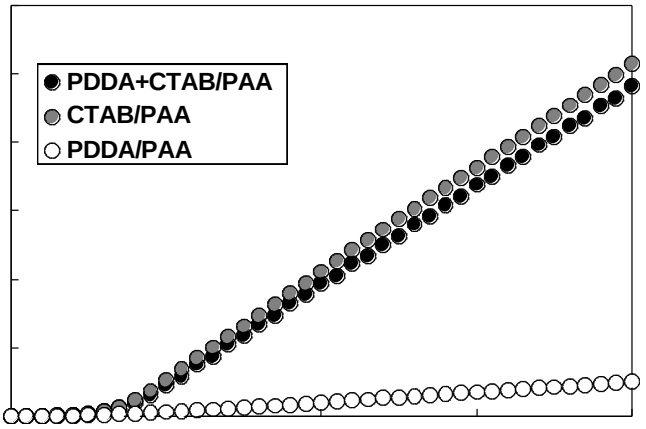

Figure 6. Quartz crystal microbalance analysis of the LbL films shows a substantial increase in film

thickness with the addition of an antimicrobial agent (adapted from Ref. 14).

Kirby Bauer tests were run under a variety of conditions to determine film effectiveness, as shown in Figure 7. One item of interest was whether or not the antimicrobial agent diffused out of only the top bilayer or if it diffused ~~through~~ throughout the system. By testing various films with different numbers of bilayers, the ability of the bottom layers to contribute to the overall antimicrobial action was shown (Fig. 7(a)). Additionally, the effect of the final anionic layer was examined by omitting it, leaving the ultimate layer the antimicrobial, cationic layer. This did not seem to have an effect. These results demonstrate that CTAB diffuses ~~through~~ throughout the system rather than merely from the top few layers. In order to investigate the influence of the top anionic layer on the antimicrobial effect, trials were run without this last layer.

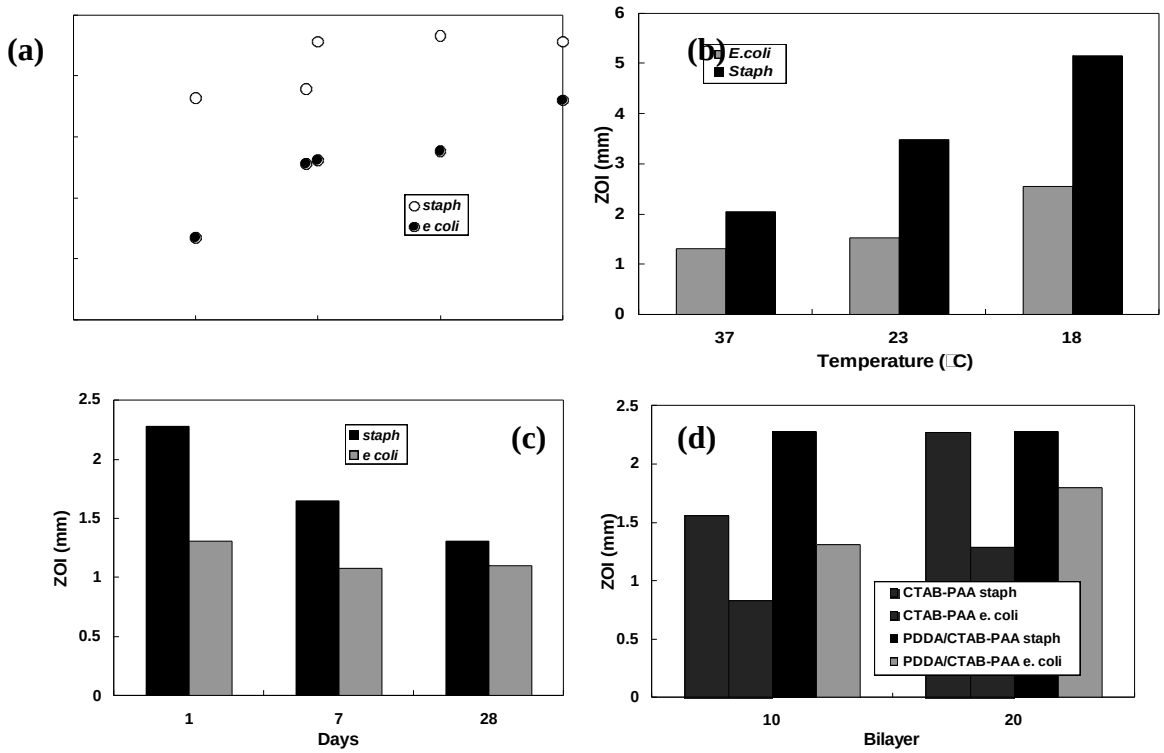

Figure 7. Kirby Bauer testing indicates an increased range of antimicrobial capabilities including (a) increased ZOI with increasing number of bilayers, (b) increasing activity with decreasing temperature, (c) decreasing effectiveness with extended time between film fabrication and testing, and (d) variations of chemistry in the cationic layer (adapted from Ref. 14).

Films were analyzed at multiple temperatures to determine the effectiveness (Fig. 7(b)). In addition to body temperature, tests were also performed at room temperature (23°C) and 18.2°C. At lower temperatures, bacteria proliferate ~~slower~~ more slowly, allowing CTAB more time to diffuse out into the KB plates before bacteria grow. With decreasing temperature, a large increase in ZOI was observed with both E. coli and Staph (Fig. 7(b)) due to the longer amount of time for CTAB to travel in the plate. The duration of the film efficacy was examined by storing the films in a dessicator for various ~~times~~ amounts of time before testing, as shown in Figure 7(c). This showed that the effectiveness does decrease initially. Over the course of a month, however, the effectiveness levels off. One explanation for this is that the film rearranges to some equilibrium state after deposition. While antimicrobial capability may not be lost, some material may settle, decreasing its ability to diffuse out. Films stored in dry environments for long periods of time may not be as potent as those used

immediately; however, these films are expected to retain antimicrobial capabilities. Finally, the antimicrobial effectiveness of both PDDA+CTAB/PAA and CTAB/PAA were evaluated. Films of both 10 and 20 bilayers were studied. In these studies, films with PDDA exhibited a greater ZOI, and thus, a greater antimicrobial efficacy (Fig. 7(d)). As is demonstrated with the microstructure, the PDDA in the cationic layer allows increased binding of CTAB in solution. With increased film stability, antimicrobial range is also increased. Solutions prepared without PDDA in the cationic layer show similar ZOI's, and could also be used in applications that do not need as large of an antimicrobial zone.

3.4 UV-resistant thin films containing colloidal TiO_2

Figure 8 shows the change in absorbance as a function of exposure time to 365 nm radiation. All three films began with sheet resistance near 30,000 Ω/square. After just 28 hours of exposure, the 12-bilayer PEI:PEDOT-PSS film experienced an order of magnitude increase in sheet resistance. The films containing TiO_2 or carbon black in their top 6 bilayers have half the sheet resistance of the unprotected PEDOT. After 270 hours, the TiO_2-containing film has only increased its resistance by ten times, while the unprotected PEDOT has increased more than 50 times. It should be noted that the film with TiO_2 was the most transparent (85% at 550 nm) of the three films.

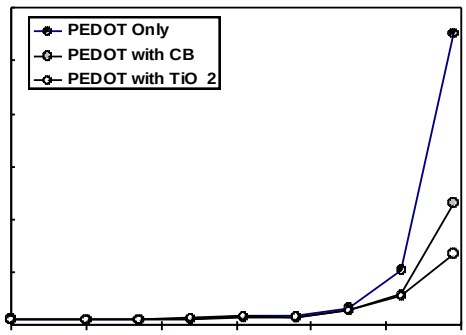

Figure 2. Oxygen transmission rate as a function of recipe at 0% and 100% RH for crosslinked and uncrosslinked, 40 bilayer, PEI (pH 10)-MMT films on 7-mil PET (adapted from Ref. 12).

Figure 9 shows the transparency of these films deposited on glass slides and placed over a penny. The film with carbon black is clearly the least transparent (%T = 67), while the TiO_2-containing film is the most transparent (%T = 86). The TiO_2 is stabilized with acetic acid and when mixed with the 0.05 wt% PEI the pH was lowered to approximately 4 (from 9 initially), thus making the PEI deposit much thinner (due to greater backbone charge density) than the unmodified, high pH PEI. Decreasing thickness with increasing charge density has been observed in layer-by-layer assemblies containing poly(acrylic acid) and polyallylamine [25]. Figure 4 shows how film growth changes for the 6-6 CB and 6-6 TiO_2 films when the particle-containing layers replace pure PEI. The initial growth for 6 bilayers on both films is almost identical. After the initial 6 bilayers, the film growth rates change dramatically. The TiO_2-containing layers grow very slowly due to the pH of the BPEI + TiO_2 solution being reduced relative to PEI alone. The carbon black + PEI layers grow at a much faster rate than the initial 6 bilayers due to the size of the carbon black clusters (100+ nm) that are being deposited. In the case of TiO_2, the 10 nm particles are individual, but the 40nm CB primary particles exist as covalently-fused clusters. Previous studies have observed large growth rates PEI-stabilized CB [26].

Figure 9. Images of 12-bilayer PEDOT-based assemblies on glass slides placed over a penny to highlight the disparity between films containing carbon black or TiO2 nanoparticles in their final 6 bilayers (adapted from Ref. 12).

4. Conclusions

Clay-filled thin films, prepared using layer-by-layer assembly, are potentially useful as foil replacement for food packaging due to their low OTR, optical transparency, and microwaveability. Despite this promise, more work is necessary to reduce moisture sensitivity and the number of bilayers required to achieve such low OTR values. This same technology may also be useful for scratch resistant surfaces or flame suppression on complex substrates (e.g., foam). Additionally, these clay-based assemblies are being studied for use as dielectric interlayers for ultrathin capacitors. PEDOT and nanotube-based assemblies are potentially useful for a variety of sensing, actuation, shielding, and memory applications. Traditional photolithographic patterning could be used on these films to further extend their capabilities. Assemblies containing quaternary ammonium salts could be useful for generating antiseptic wound dressings or antibacterial food packaging. Each of these represents an example of the overall power of the layer-by-layer assembly methodology, which should really be thought of as a technology platform on which many new applications could be developed, especially on flexible plastic film.

5. Literature citations

1. Bertrand, P., A. Jonas, A. Laschewsky and R. Legras (2000), "Ultrathin polymer coatings by complexation of polyelectrolytes at interfaces: suitable materials, structure and properties" *Macromolecular Rapid Communications*, v. 21, pp. 319-348.
2. Hammond, P. T. (2004), "Form and function in multilayer assembly: New applications at the nanoscale" *Advanced* Materials, v. 16, pp. 1271-1293.
3. Nolan, C. M., M. J. Serpe, and L. A. Lyon (2004), "Thermally modulated insulin release from microgel thin films". Biomacromolecules, v. 5, pp. 1940-1946.
4. Kim, J. H., S. H. Kim, and S. Shiratori (2004), "Fabrication of nanoporous and hetero structure thin film via a layer-by-layer self assembly method for a gas sensor" *Sensors and Actuators B*, v. 102, pp. 241-247.

5. DeLongchamp, D. M. and P. T. Hammond (2004), "Highly ion conductive poly(ethylene oxide)-based solid polymer electrolytes from hydrogen bonding layer-by-layer assembly" Langmuir, v. 20, pp. 5403-5411.
6. Yao, G. J., B. Q. Wang, Y. P. Dong, M. F. Zhang, Z. H. Yang, Q. L. Yao, L. J. W. Yip, and B. Z. Tang (2004), "Self-assembly and photovoltaic properties of multilayer films based on partially doped polyaniline and poly (4-carboxyphenyl) acetylene" *Journal of Polymer Science Part A-Polymer Chemistry*, v. 42, pp. 3224-3229.
7. von Klitzing, R. and B. Tieke (2004), "Polyelectrolyte membranes". *Polyelectrolytes with Defined Molecular Architecture I*, v. 165, pp. 177-210.
8. Etienne, O., C. Gasnier, C. Taddei, J. C. Voegel, D. Aunis, P. Schaaf, M. H. Metz-Boutigue, A. L. Bolcato-Bellemin, and C. Egles (2005), "Antifungal coating by biofunctionalized polyelectrolyte multilayered films" *Biomaterials*, v. 26, pp. 6704-6712.
9. Li, Y. C., J. Schulz, and J. C. Grunlan (2009), "Polyelectrolyte/Nanosilicate Thin-Film Assemblies: Influence of pH on Growth, Mechanical Behavior, and Flammability" *ACS Applied Materials & Interfaces*, v. 1, pp. 2338-2347.
10. Walton, M. D., Y. S. Kim, C. J. Jan, E. P. McConnell, W. N. Everett, and J. C. Grunlan (2007), "Deposition and patterning of carbon black thin films" *Synthetic Metals*, v. 157, pp. 632-.
11. Park, Y. T., A. Ham, and J. C. Grunlan (2010), "High Electrical Conductivity and Transparency in Deoxycholate-Stabilized Carbon Nanotube Thin Films" *Journal of Physical Chemistry C*, in press.
12. Dawidczyk, T. J., M. D. Walton, W. S. Jang, and J. C. Grunlan (2008), " Layer-by-layer assembly of UV-resistant poly(3,4-ethylenedioxythiophene) thin films" *Langmuir*, v. 24, pp. 8314-.
13. Grunlan, J. C., J. Choi, A. Lin (2005), "Antimicrobial behavior of polyelectrolyte multilayers containing cetrimide and silver" *Biomacromolecules*, v. 6, pp. 1149-.
14. Dvoracek, C. M., G. Sukhonosova, M. J. Benedik, and J. C. Grunlan (2009), "Antimicrobial Behavior of Polyelectrolyte-Surfactant Thin Film Assemblies" *Langmuir*, v. 25, pp. 10322-10328.
15. Jang, W. S., I. Rawson, and J. C. Grunlan (2008), "Layer-by-layer assembly of thin film oxygen barrier" *Thin Solid Films*, v. 516, pp. 4819-.
16. Priolo, M. A., D. Gamboa, and J. C. Grunlan (2010), " Transparent clay-polymer nano brick wall assemblies with tailorable oxygen barrier" *ACS Applied Materials & Interfaces*, v. 2, pp. 312-320.
17. Ploehn, H. J.; Liu, C. Y., "Quantitative analysis of montmorillonite platelet size by atomic force microscopy". *Industrial & Engineering Chemistry Research* **2006,** *45* (21), 7025-7034.
18. Owens, D. K., "Mechanism of Corona-Induced Self-Adhesion of Polyethylene Film". *Journal of Applied Polymer Science* **1975,** *19* (1), 265-271.
19. Zhang, D.; Sun, Q.; Wadsworth, L. C., "Mechanism of corona treatment on polyolefin films". *Polymer Engineering and Science* **1998,** *38* (6), 965-970.
20. Geddes, N. J.; Paschinger, E. M.; Furlong, D. N.; Caruso, F.; Hoffmann, C. L.; Rabolt, J. F., "Surface Chemical Activation of Quartz-Crystal Microbalance Gold Electrodes - Analysis by Frequency Changes, Contact-Angle Measurements and Grazing Angle Ftir". *Thin Solid Films* **1995,** *260* (2), 192-199.
21. Jang, W. S. and J. C. Grunlan (2005), "Robotic dipping system for layer-by-layer assembly of multifunctional thin films" *Review of Scientific Instruments*, v. 76, Art. No. 103904.
22. Gamboa, D., M. A. Priolo, A. Ham, and J. C. Grunlan (2010), "Influence of rinsing and drying routines on growth of multilayer thin films using automated deposition system" *Review of Scientific Instruments*, v. 81, Art. No. 036103.
23. International, A., ASTM D3985 - 05 Standard Test Method for Oxygen Gas Transmission Rate Through Plastic Film and Sheeting Using a Coulometric Sensor. West Conshohocken, PA, 2005.
24. Schlenoff, J. B., H. Ly, M. Li (1998), "Charge and mass balance in polyelectrolyte multilayers" *Journal of the American Chemical Society*, v. 120, pp. 7626-7634.

25. Shiratori, S. S. and M. F. Rubner (2000), " pH-dependent thickness behavior of sequentially adsorbed layers of weak polyelectrolytes" *Macromolecules*, v. 33, pp. 4213-4219
26. Jan, C. J., M. D. Walton, E. P. McConnell, W. S. Jang, Y. S. Kim, and J. C. Grunlan (2006), " Carbon black thin films with tunable resistance and optical transparency" *Carbon*, v. 44, pp. 1974-1981.

Acknowledgements

Special thanks ~~are paid~~ go to the Dow Chemical Company, Army Research Office, Appleton, 3M (through their Untenured Faculty Grant program), Army Research Lab, and Texas Engineering Experiment Station for financial support of various aspects of the work presented here. The student co-authors of References 9 – 16 and 26 are also thanked for their hard work and ingenuity in making these studies a success.